Bioactive imidamide-based compounds targeted against nitric oxide synthase

Fabio Arias [a], Francisco Franco-Montalban [a], Miguel Romero [b,c], Juan Duarte [b,c,d], M. Dora Carrión [a,*,1], M. Encarnación Camacho [a,*,1]

[a] Departamento de Química Farmacéutica y Orgánica, Facultad de Farmacia, Universidad de Granada, Spain
[b] Departamento de Farmacología, Facultad de Farmacia y Centro de Investigación Biomédica (CIBM), Universidad de Granada, Spain
[c] Instituto de Investigación Biosanitaria de Granada, ibs.GRANADA, Granada, Spain
[d] Ciber de Enfermedades Cardiovasculares (CIBERCV), Spain

ARTICLE INFO

ABSTRACT

The selective inhibition of inducible nitric oxide synthase (iNOS) has become an interesting goal for the treatment of diseases where the immune and inflammatory response of the organism is involved. Septic shock is one prominent example of this type of affections. In this paper, the design and synthesis of twelve substituted pyridinyl- imidamide derivatives is described, together with their biological evaluation as NOS inhibitors. The most potent and selective compound was N-(3-hydroxy-3-(pyridin-3-yl)propyl)acetimidamide 9a (IC$_{50}$ = 4.6 μM, against iNOS). Pharmacological assays in aortic rat tissue, have confirmed its inhibitory activity on iNOS and the absence of undesired cardiovascular effects. In silico analysis of the most promising compounds (9a, 9b, 9e and 9g) have predicted good drug-likeness properties. Furthermore, they have shown an adequate cell viability. Docking studies carried out on 9a suggest a particular binding mode that involves the essential residue Glu377, and might explain its iNOS selectivity. From a chemical point of view, the article describes an unusual cyclization to obtain pyridinyl-pyrimidine derivatives with high yield.

1. Introduction

Nitric oxide (NO) is a heterodiatomic molecule formed by oxygen and nitrogen, this free radical plays a key role in several neurotransmission pathways and in the regulation of immune and cardiovascular systems [1].

In the organism, NO is synthesized after L-arginine is transformed into L-citrulline with the consumption of NADPH and O_2. This reaction is catalysed by the Nitric Oxide Synthase (NOS), an family of enzymes which is present in three different isoforms depending on their location: nNOS, the neuronal isoform [2], eNOS, the endothelial isozyme [3] and iNOS the inducible one [4]. This last isozyme can be expressed in almost any cell of the organism if the proper signal is received [5].

The two main roles of NO in the cardiovascular system are relaxing the muscular smooth tissue and reducing platelet aggregation. After being synthesized in the endothelium, NO is able to diffuse through the cellular membrane to the adjacent muscular tissue [6]. There, it activates guanilate cyclase unchaining the GMPc signalling, decreasing intracellular levels of Ca which results in vascular tone relaxation [7].

Since NO is involved in such variety of systems, alterations in NOS activity take part in the development of many pathologies, such as, schizophrenia [8], neurodegenerative diseases [9-11], several types of cancer [12,13], migraine [14] and septic shock [15].

Among these, we will focus specifically in septic shock, the most drastic organism response against systemic infection [16]. After contamination and propagation of pathogens in blood (usually bacteria), the human body enters in sepsis. This state activates the immune response, inducing the expression of iNOS in macrophages, endothelium and in the muscular smooth tissue wrapping the blood vessels. This results in very high levels of NO that drop the blood pressure to ranks unable of irrigate the organs leading to multiorganic failure [17].

The survival rate for this complication is around 50% even after treatment with vasopresors [18]. An interesting approach to reduce the number of deceases could be the inhibition of NOS inducible isoform, maintaining the endothelial one active. This implicates that vasodilation would be slowed down without exceeding the basal vasoconstriction

* Corresponding authors.
E-mail addresses: dcarrion@ugr.es (M. Dora Carrión), ecamacho@ugr.es (M. Encarnación Camacho).
[1] These authors contributed equally.

tone.

Throughout the last years, our research group has collected several examples of selective nNOS and iNOS inhibitors, including derivatives with a heterocyclic ring, as 2,3-dihydro-1,3,4-thiadiazoles **1** [19], and 4,5-dihydro-1*H*-pyrazoles **2** [20,21], or compounds with a flexible chain, as the ureas and thioureas **3** [22,23], or the imidamides (**4**, **5**) [24] with interesting NOS inhibition values (Fig. 1).

On the other hand, according to literature, the pyridine ring is a recurrent feature in several NOS inhibitors, as the 6-(4-(substituted) phenyl)-2-aminopyridines **6** [25], and the symmetric double-headed aminopyridines **7** [26], both types with selectivity versus the neuronal NOS, or the substituted 2-aminopyridines **8** [27], some of which showed potency and specificity for the inducible isoform (Fig. 2).

In this paper, we report the synthesis and biological evaluation of a series of analogues with a pyridine ring and an imidamide scaffold in their skeleton. Pyridinyl-imidamides **9a-d** and **10a** have been designed from the phenyl-imidamides **4** and **5**, respectively, by isosteric replacement of their benzene ring with a pyridine one. In addition, dimers **9e-g** come from the molecular duplication of two *N*-(3-hydroxy-3-(pyridin-3-yl)propyl)imidamide scaffolds, linked by oxygen (imidocarbamate **9e**) or NH (biguanidine **9f**), or without linker (guanidine **9g**). In addition, molecules **11a-d** with a pyridinyl-pyrimidine skeleton, derived from an unusual cyclization of the pyridinyl-imidamides **9a-d**, have also been synthesised (Figs. 3 and 4).

2. Results and discussion

2.1. Chemistry

The general synthetic pathway to achieve the final derivatives **9a-d**, **10a** and **11a-d** is summarized in Scheme 1. Nicotinaldehyde **12** was treated with acetonitrile and *n*-BuLi in dry THF to give rise the β-hydroxinitrile **13** (94% yield). The nitrile group of this last compound was reduced to the primary amine **14** by adding LiAlH₄ in THF. Compound **14** was used without further purification due to its chemical instability. Next, commercially available ethyl acetimidate hydrochloride **15a** or the previously synthesized benzyl benzimidothioates **15b-**

d (79–94% yield) were added to the 3-amino-1-(pyridin-3-yl)propan-1-ol to give the final *N*-(3-hydroxy-3-(pyridin-3-yl)propyl)imidamides **9a-d** (80–98% yield). For the synthesis of *N*-(3-oxo-3-(pyridin-3-yl)propyl) acetimidamide **10a** (61% yield), the hydroxyl group of **9a** was oxidized to a carbonyl function, using a mixture of sodium dichromate and sulfuric acid in aqueous medium. Due to synthetic problems that arose while oxidating **9a**, only the first member of the series was obtained. The moderate yield in the oxidation reaction might be due to the presence of the pyridine ring. The slightly basic character of the pyridine ring and the presence of chromic acid induced the formation of adducts in which the *N*-Cr bond is involved. Therefore, we decided to replace the oxidizing agent with MnO₂. In this way, the imidamides **9a-d** were treated with manganese dioxide in acetonitrile leading to an unexpected cyclization of the alkyl chain and the imidamide function, which became the pyrimidine ring present in the final 2-substituted-4-(pyridin-3-yl)pyrimidine derivatives **11a-d** (80–85% yield). Although this type of derivatives have been described [28], to our knowledge, this is the first example of pyridinyl-pyrimidines synthesis from hydroxyl imidamido oxydation. The use of MnO₂ induces aromatization allowing the isolation of the final **11a-d** derivatives (Scheme 2).

In order to obtain the dimeric derivatives, it was necessary to start from the aminopropanol **14**; using cyanogen bromide, the cyanamide function was introduced, to give *N*-(3-hydroxy-3-(pyridin-3-yl)propyl) cyanamide **16** (85% yield), a key intermediate that allowed all synthetic branches for the last final products. In this way, hydration of **16** led to the *N*-(3-hydroxy-3-(pyridin-3-yl)propyl)carbamimidic acid **17** (93% yield), which in the presence of sodium hydride and an equimolar amount of cyanamide **16**, yielded the imidocarbamate **9e** (76% yield). On the other hand, treatment of cyanamide **16** with a NH₄Cl solution allowed the obtention of biguanidine **9f** (68% yield), probably via the not isolated intermediate 1-(3-hydroxy-3-(pyridin-3-yl)propyl)guanidine **18**. Finally, the cyanamide **16**, in the presence of the aminopropanol hydrochloride **14**, yielded the final guanidine **9g** (73% yield) [29] (Scheme 3).
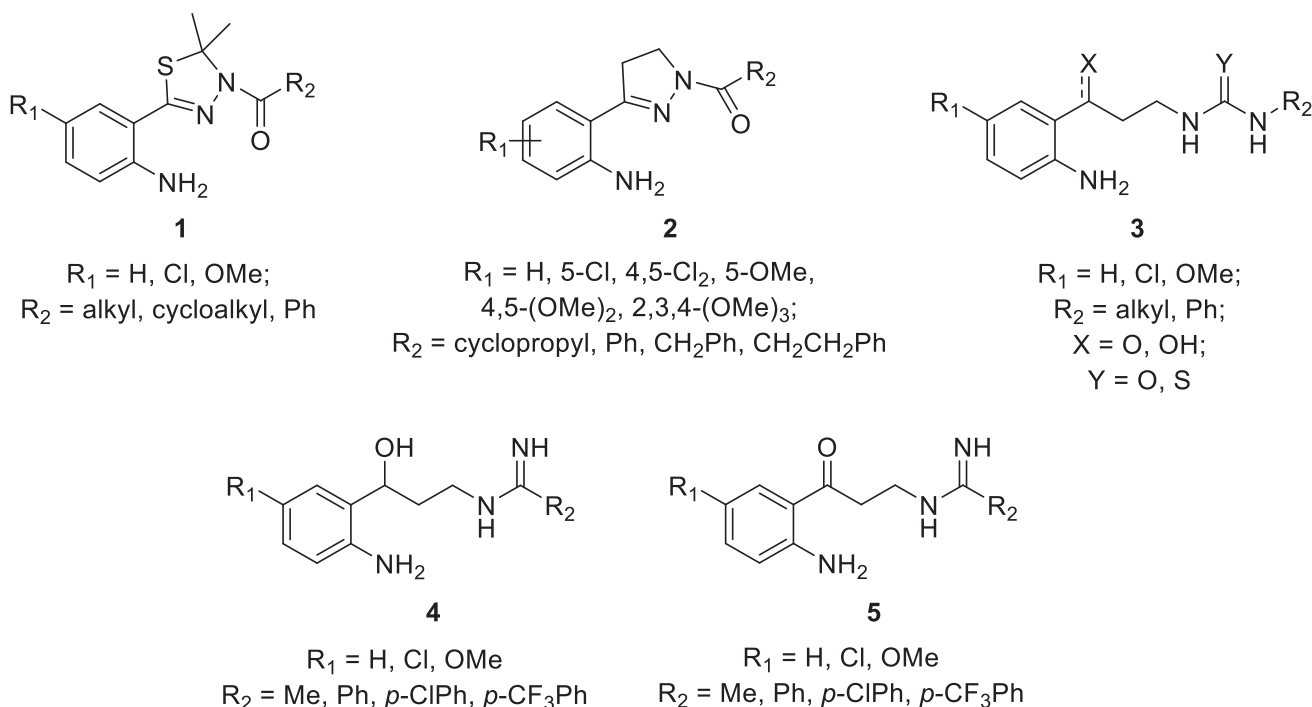

Fig. 1. Diverse NOS inhibitors synthesized by our research group.

1

R₁ = H, Cl, OMe;
R₂ = alkyl, cycloalkyl, Ph

2

R₁ = H, 5-Cl, 4,5-Cl₂, 5-OMe,
4,5-(OMe)₂, 2,3,4-(OMe)₃;
R₂ = cyclopropyl, Ph, CH₂Ph, CH₂CH₂Ph

3

R₁ = H, Cl, OMe;
R₂ = alkyl, Ph;
X = O, OH;
Y = O, S

4

R₁ = H, Cl, OMe
R₂ = Me, Ph, *p*-ClPh, *p*-CF₃Ph

5

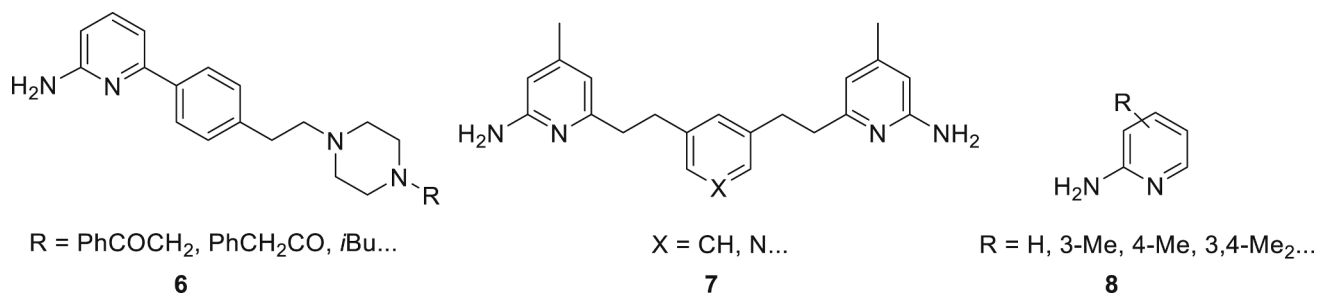R₁ = H, Cl, OMe
R₂ = Me, Ph, *p*-ClPh, *p*-CF₃Ph

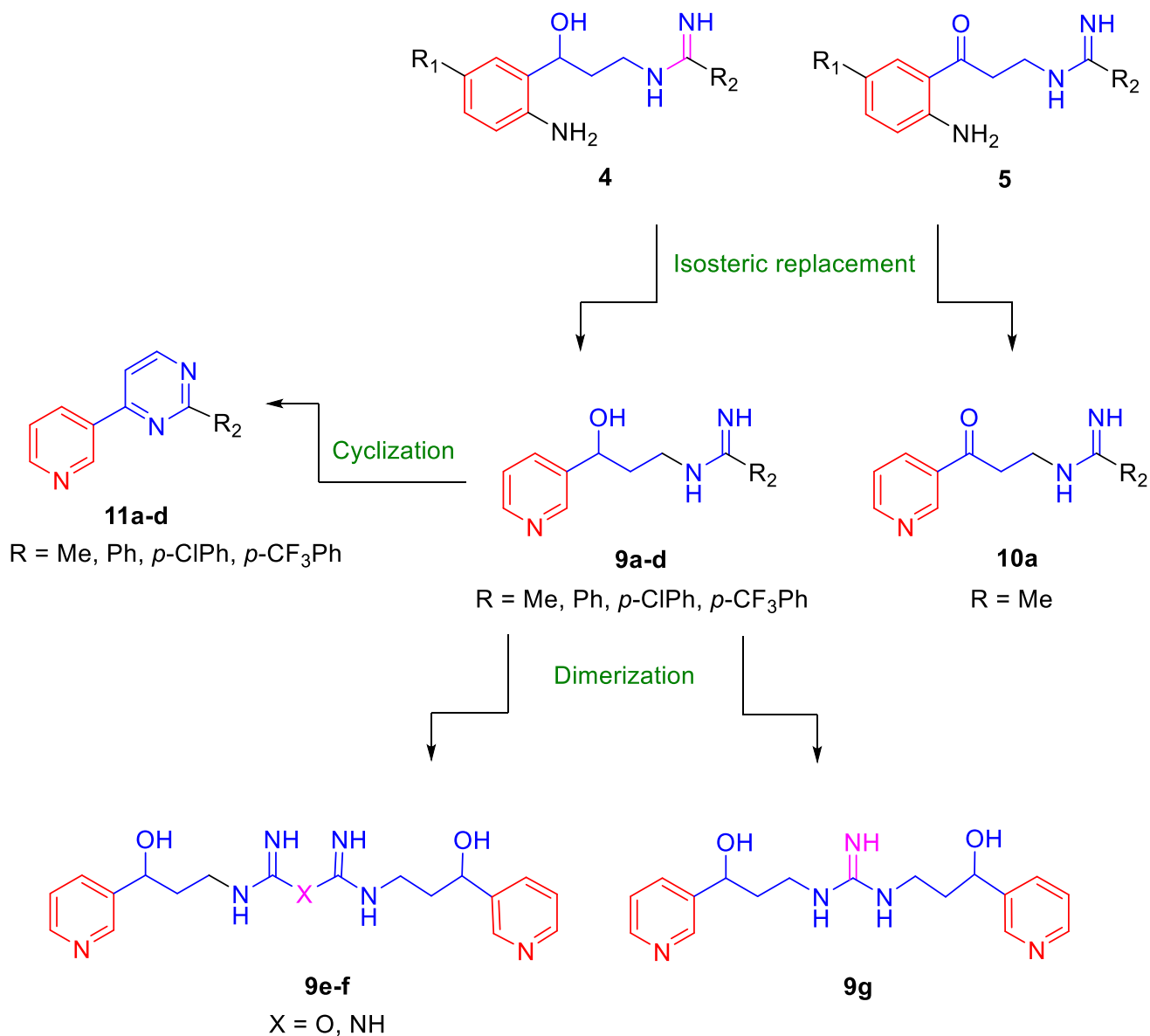Fig. 2. Examples of NOS inhibitors with a pyridine ring.

Fig. 3. Design strategy of new imidamide-based molecules synthesized by our research group.

2.2. Biological activity evaluation

2.2.1. iNOS and nNOS inhibition

In order to determine the inducible and neuronal NOS isoforms inhibitory activity percentages of these derivatives, first, we carried out a screening using recombinant iNOS and nNOS enzymes. The results are collected in Table 1, among all compounds, those with the best inhibition values (**9a-b**, **9e** and **9g**), were selected to calculate their IC_{50} and the resulting data are included in Table 2.

Regarding the imidamide series (**9a-d** and **10a**), the iNOS inhibition percentages fluctuate between 13.28% and 94.02%, while those of nNOS oscillate within 13.08% and 69.44%, the selectivity towards iNOS being greater in the hydroxypropyl compounds, whilst the only candidate with a carbonyl group shows a higher percentage of nNOS
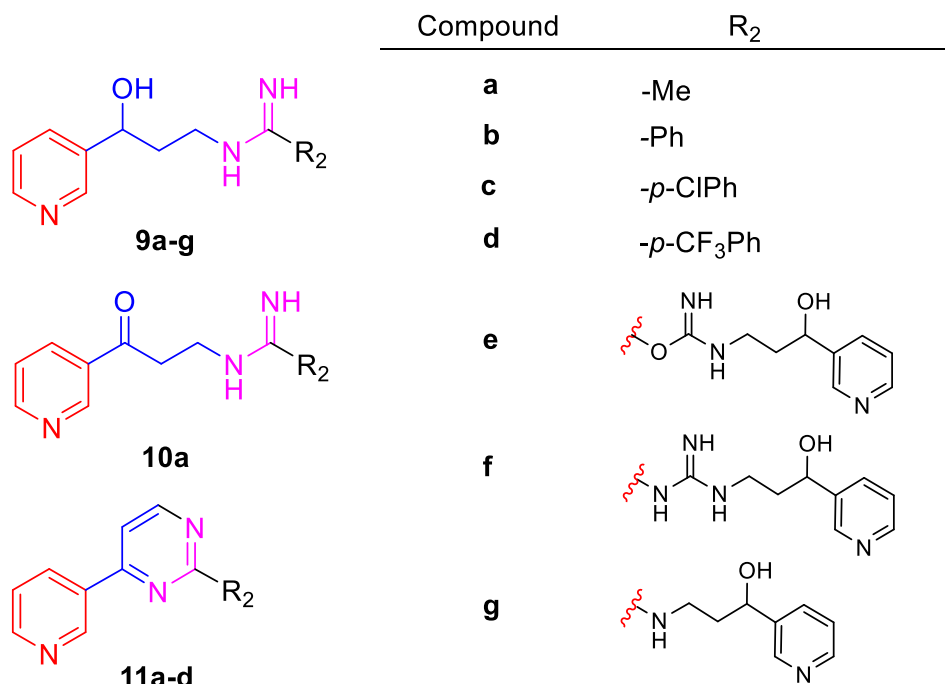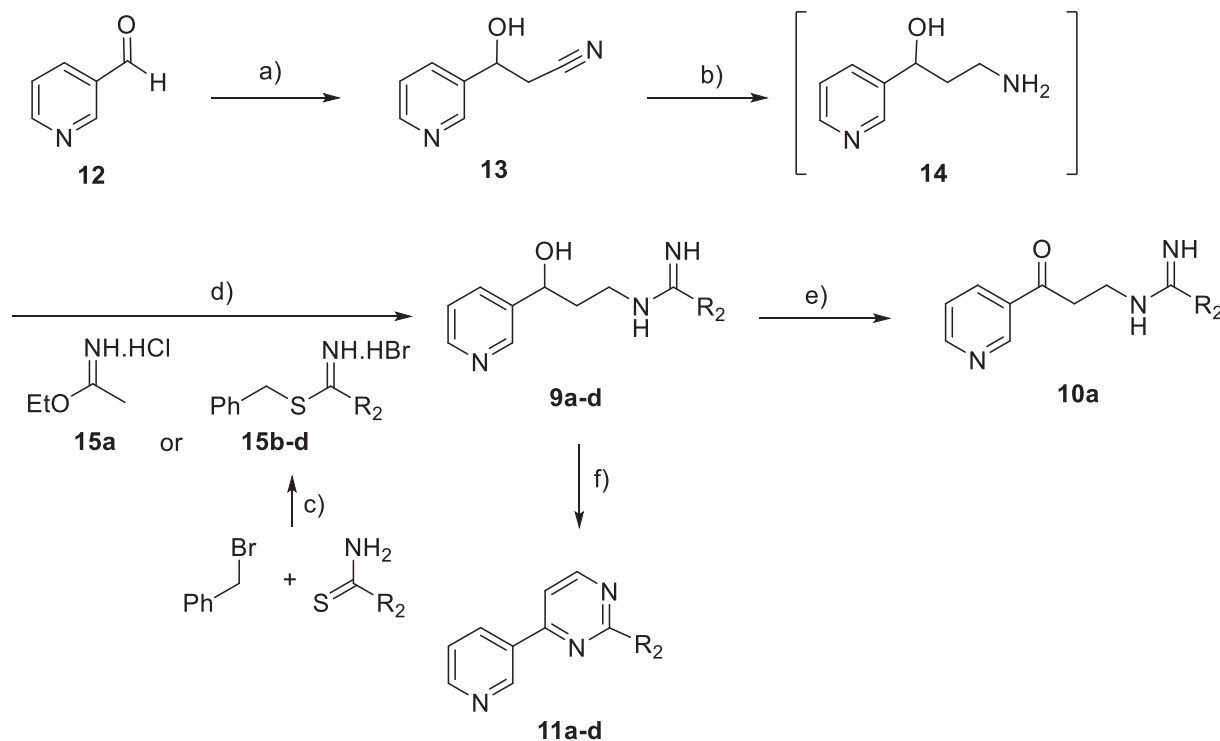
Compound	R$_2$
a	-Me
b	-Ph
c	-*p*-ClPh
d	-*p*-CF$_3$Ph
e	
f	
g	

Fig. 4. Structure of the novel synthesized imidamide-based derivatives.


Scheme 1. Synthetic route of pyridinyl-imidamides **9a-d** and **10a**, and pyridinyl-pyrimidines **11a-d**. Reagents and conditions: a) CH$_3$CN, BuLi, THF, −78 °C, 30 min, then RT; b) LiAlH$_4$, THF, 0 °C, 20 min; c) CHCl$_3$, reflux 2 h; d) MeOH 0 °C, then 15 h RT; e) Na$_2$Cr$_2$O$_7$, H$_2$O, 0 °C; then 10 M H$_2$SO$_4$, 16 h; f) CH$_3$CN, MnO$_2$, 48 h RT.

inhibition (about 70%). Of all compounds tested, **9a** was the best inhibitor, presenting an IC$_{50}$ value of 4.6 μM and a selectivity of more than 200 times over nNOS. Compound **9b** also showed a good IC$_{50}$ value in iNOS (76.0 μM) and good iNOS selectivity (Table 2).

Derivatives **9a-d** and **10a** have been designed from imidamides **4** and **5**, respectively, by isosteric replacement of a phenyl ring by a pyridine heterocycle, being **4a** (R$_1$ = OMe, R$_2$ = *p*-CF$_3$Ph; IC$_{50}$ = 20.0 μM) the most active molecule of the hydroxypropyl series, and **5a** (R$_1$ = Cl,

R$_2$ = Me; IC$_{50}$ = 25.6 μM) the best iNOS inhibitor of the oxopropyl family. As we can see in Table 2, the pyridine isosteric substitution improves the iNOS activity over hydroxypropyl derivatives, maintaining the iNOS/nNOS selectivity.

In relation to the dimeric derivatives (**9e-g**), the preliminary screening showed a greater selectivity towards iNOS with values ranging between 65.48% and 93.93% (Table 1). Compounds **9e** and **9g**, with the highest iNOS inhibition percentages in this family, were selected to
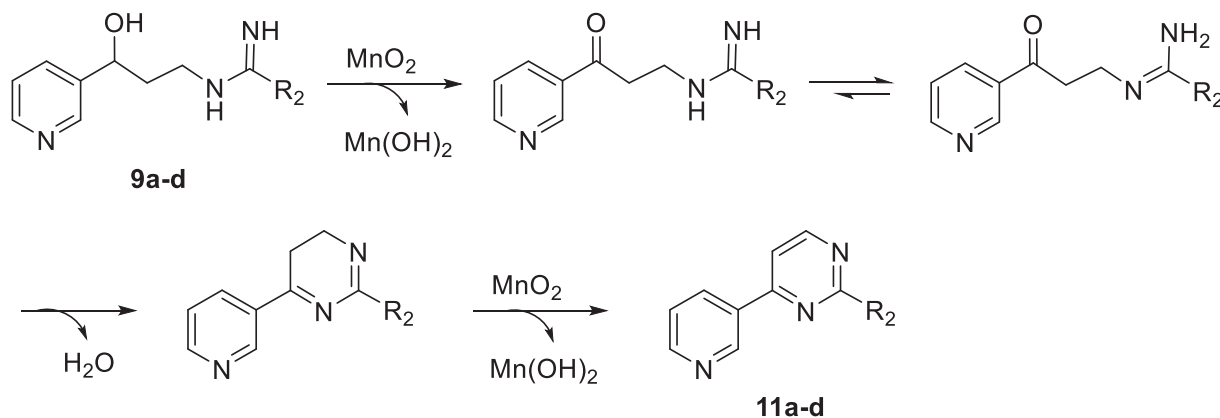
Scheme 2. Proposed mechanism for the cyclization of pyridin-pyrimidines **11a-d**.
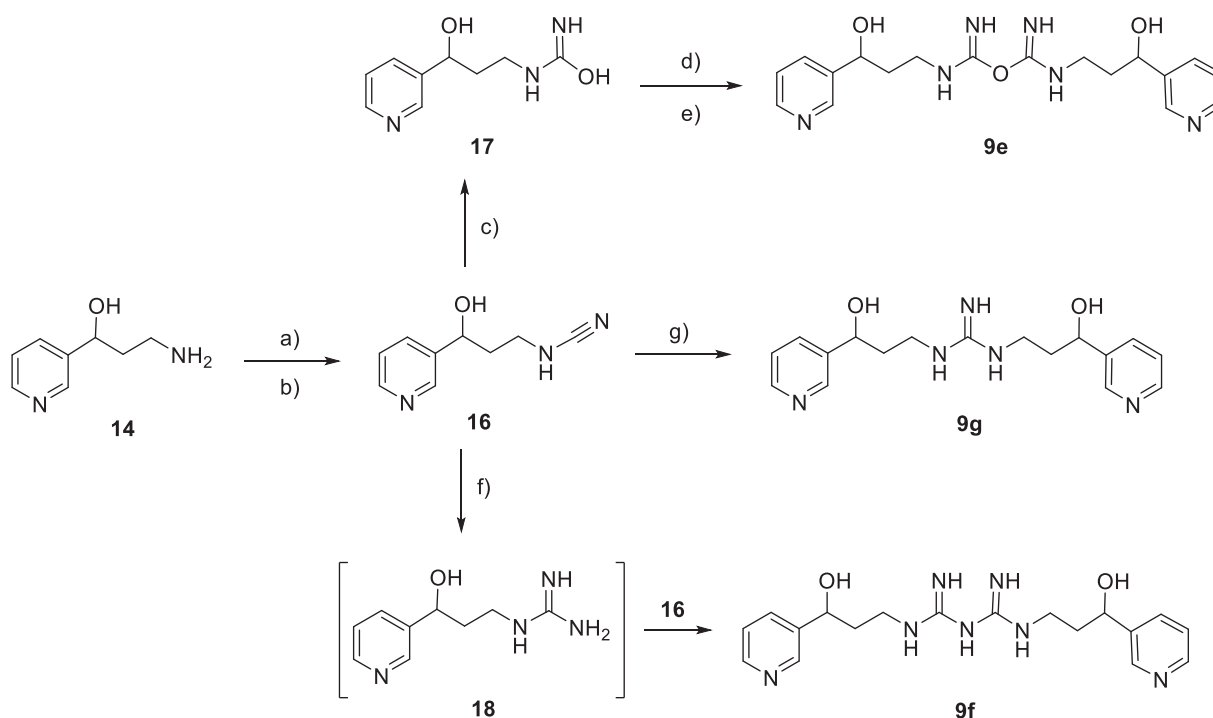
Scheme 3. Synthetic route for imidocarbamate **9e**, biguanidine **9f** and guanidine **9g**. Reagents and conditions: a) MeOH, NaOAc; b) BrCN, 0 °C, then 2 h RT; c) H$_2$O; d) DMSO, NaH, 1 h RT; e) **16**, 24 h RT; f) DMF, 1 M NH$_4$Cl, 1 h reflux, then 2 M NaOH; g) EtOH, then **14**·HCl, 3 h reflux.

calculate their IC$_{50}$. In this sense, guanidine **9g** was the most powerful dimer with IC$_{50}$ = 46.9 μM in iNOS (Table 2).
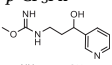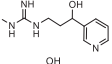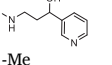
On the other hand, regarding the pyrimidine series (**11a-d**), the preliminary *in vitro* study shows that the inhibition values shift between 0.29% and 67.85% for iNOS, while those of nNOS are between 30.44% and 63.00%. The preference of this family of compounds for nNOS is higher when compared to the previously studied families. In this series, **11d** (R$_2$ = *p*-CF$_3$Ph) was the one with higher inhibition percentage in both isoforms.

2.2.2. Effects of 9a on LPS-induced vascular hypo-reactivity to noradrenaline and eNOS inhibition

The imidamide **9a** is the most interesting compound in this family due to it was the best iNOS inhibitor. Hence, in order to test functional evidence and to ensure the iNOS selectivity of this compound, we performed a pharmacological assay, using descending thoracic aortic rings without endothelium. A vascular hyporeactivity to noradrenaline (NA) induced by endotoxin (lipopolysaccharide, LPS) was described

previously [30]. This effect is related to an enhanced NO production by activation of iNOS in vascular smooth muscle. In fact, a selective inhibitor of iNOS, aminoguanidine, reversed the blunted phenylephrine-evoked contraction of endothelium-denuded aortic rings from LPS-treated rats or rings exposed to LPS *in vitro*. However, aminoguanidine did not impair the eNOS-dependent relaxation to acetylcholine in aortic rings with endothelium [31]. Similarly, we observe that incubation of LPS reduced the contractile responses elicited by NA in aortic rings without endothelium (approximately 73% AUC), as shown in Fig. 5A. Incubation of endothelium-denuded aortic rings with NG-nitro-L-arginine methyl ester (L-NAME), a potent inhibitor of NO synthesis, significantly restored NA responses from LPS incubated aortic rings, showing that NO is involved in the attenuated vascular reactivity to NA induced by endotoxin (Fig. 5C). Furthermore, the presence of the **9a** prevented endotoxin-induced contractile hyporesponsiveness to NA, in a similar extension than L-NAME (Fig. 5C). However, **9a** was unable to modify the contractile response to NA in control rings (without activation of iNOS by LPS) (Fig. 5B), showing that this compound improved NA contraction

Table 1

In vitro iNOS and nNOS inhibition (%) observed of compounds **9a-g**, **10a** and **11a-d**.

Compound	R₁	R₂	% iNOS inhibition[a]	% nNOS inhibition[a]
9a	–	-Me	92.49 ± 1.49	13.08 ± 2.59
9b	–	-Ph	94.02 ± 1.97	20.53 ± 2.07
9c	–	*-p*-ClPh	77.90 ± 1.87	53.61 ± 1.80
9d	–	*-p*-CF₃Ph	28.98 ± 0.87	12.27 ± 0.39
9e	–	(structure)	88.43 ± 1.53	21.65 ± 0.55
9f	–	(structure)	65.48 ± 2.30	7.87 ± 2.59
9g	–	(structure)	93.93 ± 0.15	69.29 ± 0.55
10a	–	-Me	13.28 ± 1.78	69.44 ± 0.47
11a	–	-Me	26.78 ± 0.84	57.15 ± 1.28
11b	–	-Ph	0.29 ± 0.42	45.66 ± 2.13
11c	–	*-p*-ClPh	33.30 ± 3.36	30.44 ± 4.27
11d	–	*-p*-CF₃Ph	67.85 ± 3.87	63.00 ± 4.41
4a[b]	-OMe	*-p*-CF₃Ph	99.61 ± 0.55	12.50 ± 1.06
5a[b]	-Cl	-Me	99.14 ± 0.69	19.88 ± 0.57

[a] Values are the mean ± SEM of the percentage of iNOS and nNOS inhibition produced by 1 mM concentration of each compound. Each value is the mean of three experiments performed by triplicate using recombinant iNOS and nNOS enzymes.

[b] **4a** and **5a** [24] were used as reference.

Table 2

IC₅₀ values (μM) for the iNOS and nNOS inhibition activity by compounds **9a-b**, **9e**, **9g**.

Compound	iNOS	nNOS
9a	4.6	> 1000
9b	76.0	> 1000
9e	107.6	> 1000
9g	46.9	> 1000
4a[b]	20.0	> 1000
5a[b]	25.6	> 1000

[a] Data obtained by measuring the percentage of inhibition with at least six concentrations of the inhibitor.

[b] Imidamides **4a** and **5a** [24] were used as reference.

in vascular smooth muscle by iNOS inhibition.

We also carried out the eNOS inhibitory activity of **9a**, using a functional test. In this way, acetylcholine (Ach)-induced endothelium-dependent relaxation has been analyzed using endothelium intact rat aortic rings. This classic cholinergic agonist activates eNOS by a calcium-dependent mechanism [32]. The endothelium-dependent relaxation to acetylcholine was not affected by **9a** (Fig. 6), confirming the absence of eNOS inhibition of this compound, whereas the non-selective NOS inhibitor ʟ-NAME almost abolished this response.

2.2.3. Cell viability

We investigated the cell viability activity of compounds **9a**, **9b**, **9e** and **9g** using HUVECs. The tested concentrations were within the range of IC₅₀ values for the inhibition of iNOS activity by the most potent imidamide derivatives. We observed that these compounds have little toxicity, since only at higher concentration tested (above 100 μM), the cell viability is significantly (approximately 20%) reduced (Fig. 7).

2.3. Molecular docking study

Based on their IC₅₀ values, compounds **9a** and **9g** were selected for docking studies. These compounds show a significant iNOS selectivity over nNOS, hence, determining their molecular interactions in both isozymes would help in understanding their mechanism of action and might benefit in the design of more potent chemical derivatives. PDB IDs

4CX7 and 6AV2, corresponding to human iNOS and nNOS, respectively, were selected as candidates to assess the molecular interactions of both compounds. These two PDB files present 2-aminopyridine inhibitors bind to their catalytic active site. Redocking of the cognate ligands on crystal structures 4CX7 and 6AV2 were carried out to account for the validity of docking protocol. In both cases, the preferred poses for the cognate ligands matched those of the crystal structures (see supporting information). The preferred poses of **9a** and **9g** on hiNOS (PDB ID 4CX7) are shown on Fig. 8. As depicted, both ligands display their pyridine ring underneath the heme cofactor and perpendicular to it, with the nitrogen atom orientated toward the Fe atom. Also, a stacking interaction of the pyridine ring with Val352 is observed in both ligands. Compound **9a**, seems to tightly bind the catalytic site by H-bonding the important Glu377 residue with its imidamide moiety. Compound **9g**, on the other hand, extend its second hydroxypyridine group toward Asn354, at the entrance of the catalytic pocket, H-bonding it with the pyridinic nitrogen atom, and aromatic stacking Tyr491, a highly conserved residue of low mobility in iNOS but able to adopt an out rotamer position in nNOS and eNOS [33]. In this pose, the guanidine moiety of **9g** rest underneath the heme propionate groups and is able to double H-bond the B-propionate together with the hydroxyl group. In general, the pose compound **9g** somehow resemble the that of the cognate ligand in the crystal structure (4CX7), where its second aminopyridine ring lays at the entrance of the catalytic channel H-binding the heme B-propionate (see crystal structure PDB ID 4CX7).

On hnNOS (PDB ID 6AV2), however, the same two ligands adopt significantly different poses (Fig. 9). Ligand **9a**, the most active iNOS inhibitor, displays its pyridine ring below the heme cofactor, but instead of positioning its nitrogen atom toward the Fe atom, it establishes a H-bond with the backbone chain of Val572 (Val352 on iNOS). Moreover, its hydroxyl group is able to H-bond Glu597 (Glu377 in iNOS), while the imidanide group is displayed toward the heme propionate groups H-bonding both carboxylate groups. Compound **9g**, like **9a**, displays one of its hydroxypyridine heads below the heme cofactor, with its nitrogen atom H-bonding the backbone chain of Val572 and the hydroxyl group making a single H-bond with Glu597 (Glu377 in iNOS). Its imidamide moiety H-bond Asp602 (Asp382 in iNOS; Asn368 in eNOS), an iNOS/nNOS conserved residue, and the second hydroxypyridine head is set toward the arginine pocket (Arg486, not shown, Arg608 and Arg601) stacking Arg601.

Some potent and selective iNOS inhibitors have been published and their key interactions with specific protein residues described. Among these, bidentate H-bonds to Glu377 and stacking interactions with heme are the most significant since they involve the catalytic active site [34]. As the docking result shows (Figs. 8 and 9), ligands **9a** and **9g** are able to bind with the catalytically important residue Glu377 and heme cofactor. Of particular interest is the three point chelate-like interaction of **9a** with Glu377 in the catalytic site, which might help explaining its higher experimental IC₅₀ values and selectivity toward iNOS. Ligand **9g**, on the other hand, while binding Glu377 only with a single H-bond, is able to π-stack Tyr491, a residue that shows low mobility in iNOS, but is able to rotate in nNOS and eNOS, suggesting a higher selectivity of **9g** toward iNOS.

2.4. In silico prediction of physicochemical properties and pharmacokinetic profile

2.4.1. Physicochemical parameters

The most active compounds (**9a**, **9b**, **9e** and **9g**) have been subjected to computational studies in order to predict their basic pharmacokinetic properties using pKSCM tool (https://biosing.unimelb.edu.au/pkscm/prediction) [35]. The SMILE molecular structures of compounds were obtained from PubChem (https://pubchem.ncbi.nlm.nih.gov). Table 3 shows the predicted Lipinski and Veber parameters. As can be seen from the table, no compound violates Lipinsky's rules, and only derivative **9e** has a polar surface area that exceeds the limit value. Hence, according to
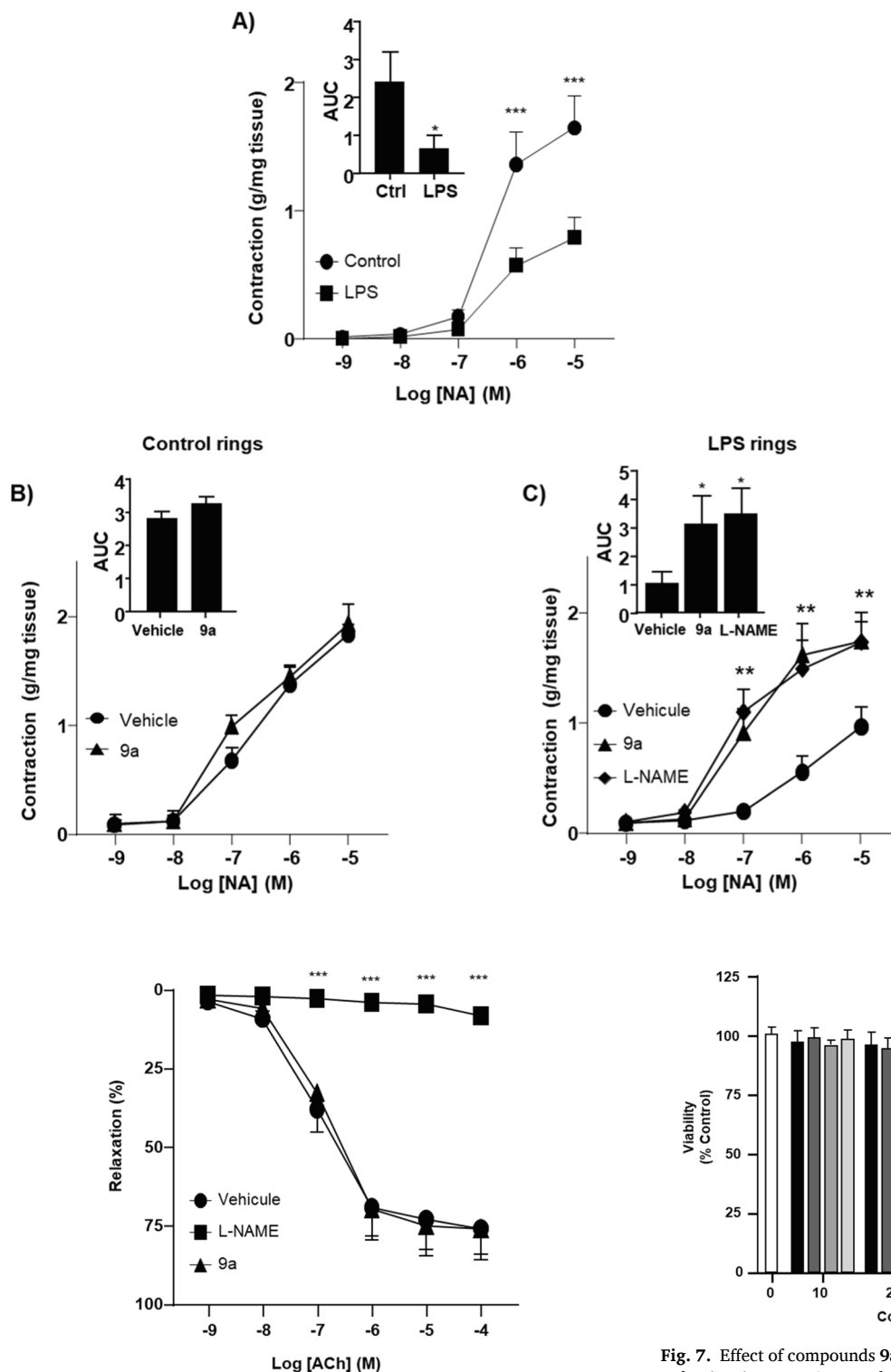
Fig. 5. Effects of 9a on noradrenaline induced contraction in LPS-treated endothelium-denuded aortic rings. NA-evoked contraction of rat aortic rings (n = 4–8) without endothelium treated *in vitro:* (A) with or without LPS (1 μg/ml, 20 h), or (B) in the presence of 9a (5 μM) or its vehicle (DMSO, 1/10⁶) 30 min before NA in untreated endothelium-denuded aortic rings, or (C) in the presence of L-NAME (300 μM), 9a (5 μM), or its vehicle (DMSO, 1/10⁶) 30 min before NA in LPS-treated endothelium-denuded aortic rings. The Area Under contraction-response Curve (AUC) was represented inside. Data are expressed as means ± standard error mean of n experiment. *P < 0.05 and ** P < 0.01 vs. LPS group, or vehicle treated rings.
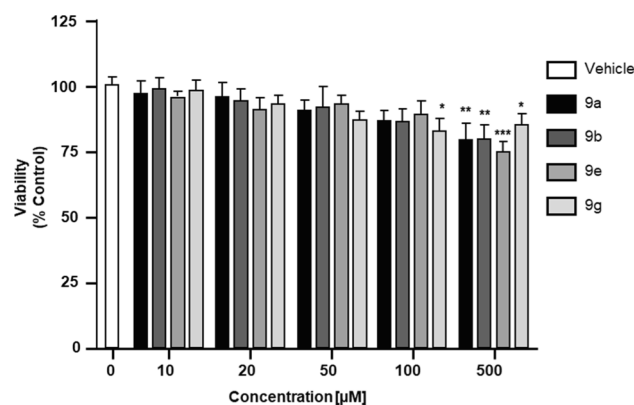

Fig. 6. Effects of compound 9a on eNOS activity. Acetylcholine (Ach)-evoked relaxation in aortic rings with endothelium contracted with 1 μmol/L NA, after incubation with L-NAME (100 μM), 9a (5 μM) or its vehicle (DMSO, 1/10⁶) for 30 min (n = 8). Data are expressed as means ± standard error mean of n experiment. ***P < 0.001 vs. rings incubated with vehicle.

Fig. 7. Effect of compounds 9a, 9b, 9e and 9g on cell viability assessed by MTT reduction in HUVECs. Results were calculated as percentage of control (untreated cells) and data are presented as mean ± standard error of the mean (SEM) (n = 3 per group). *P < 0.05, ** P < 0.01 and ***P < 0.001 vs. vehicle treated cells.

these results, it can be concluded that the tested molecules possess good drug-like properties.

2.4.2. ADME properties

In relation to the ADME properties (Table 4), they were calculated using the web http://biosig.unimelb.edu.au/pkcsm/prediction. In this way, the BBB permeability of all the compounds was considered promising as the log BB values were below 0.3, and therefore they could be safely used with minimal side effects on the CNS.

Intestinal absorption (HIA) and Caco2 permeability indices are factors that determine the ultimate bioavailability of the drug. The tested derivatives showed good human intestinal absorption effects ranging
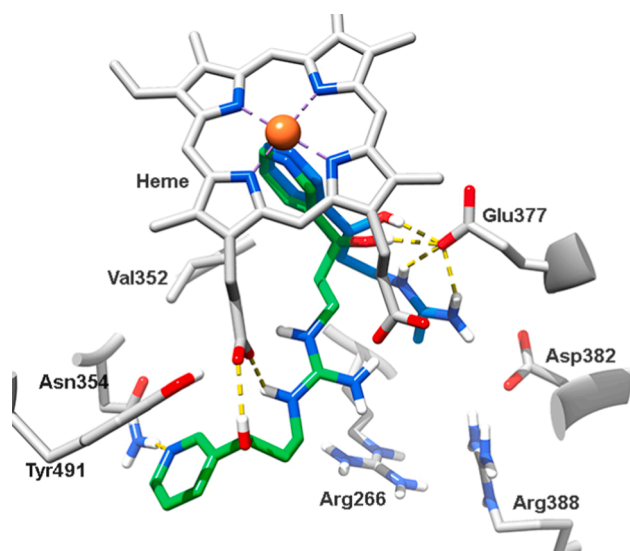
Fig. 8. Superposition of predicted binding poses of **9a** (blue) and **9g** (green) on iNOS (pdb ID 4CX7, grey). Hydrogen bonds are represented by dashed yellow lines. (For interpretation of the references to colour in this figure legend, the reader is referred to the web version of this article.)

Fig. 9. Superposition of predicted binding poses of **9a** (blue) and **9g** (green) on nNOS (pdb ID 6AV2, tan). Hydrogen bonds are represented by dashed yellow lines. (For interpretation of the references to colour in this figure legend, the reader is referred to the web version of this article.)
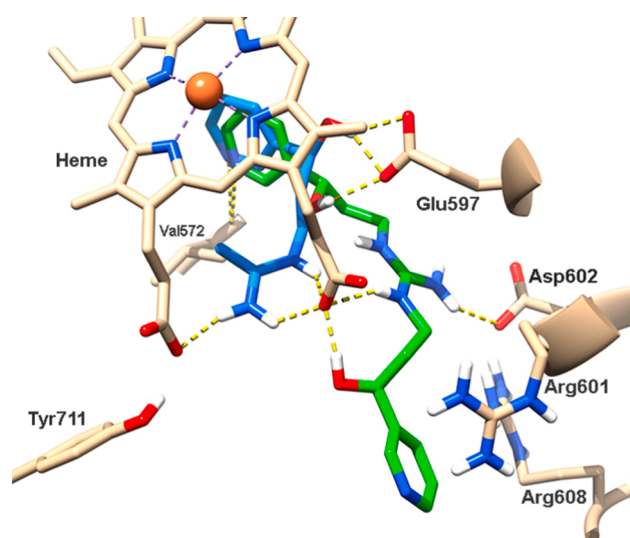
Table 3
Calculated Lipisnki and Veber parameters for compounds **9a**, **9b**, **9e** and **9g**.

Comp.	MW	LogP	HBD	HBA	nVs	nRB	MolPSA
Lipinski*	≤500	≤5	≤5	≤10	≤1	–	–
Veber**	–	–	–	–	–	≤10	≤140 Å²
9a	193.25	1.09	3	3	0	4	83.50 Å²
9b	255.32	2.12	3	3	0	5	112.20 Å²
9e	372.43	1.09	6	7	0	8	157.02 Å²
9g	329.40	1.14	5	5	0	8	140.86 Å²

* Lipinski reference values.
** Veber reference values; MW, Molecular weight; LogP, lipophilicity (O/W); HBD, Number of hydrogen bond donors; HBA, Number of hydrogen bond acceptors; nVs, Number of Lipinski rule violations; nRB, Number of rotatable bonds; MolPSA, molecular polar surface area (PSA) (Å²).

Table 4
ADME properties of **9a-b**, **9e** and **9g** derivatives.

Comp.	BBB (log BB)	HIA (%)	Caco2 (Log Papp in 10^{-6} cm/s)	CYP3A4 inhibition	CYP2C19 inhibition	AMES toxicity
9a	−0.775	66.05	0.688	No	No	No
9b	−0.569	91.55	1.133	No	Yes	No
9e	−1.730	47.33	0.171	No	No	No
9g	−1.137	58.91	−0.105	No	No	No

BBB, Blood Brain Barrier permeability; HIA, Human Intestinal absorption; Caco2, permeability through Caco-2 (human colorectal carcinoma) cells *in vitro*; CYP3A4, Cytochrome P4503A4; CYP2C19, Cytochrome P4502C19; AMES, Salmonella typhimurium reverse mutation assay.

from 47 to 91% absorption (high absorption, 70–100%; medium absorption, 20–70%), and, in general, they had relatively low Caco2 permeability potential ($<8 \times 10^{-6}$ cm/s), thus, they could be absorbed through the human intestine.

Cytochrome P4503A4 (CYP3A4) and cytochrome P4502C19 (CYP2C19) isozymes play a significant role in drug metabolism in the liver. In general, the tested compounds had no CYP interactions. Finally, predicted toxicity of drugs through AMES toxicity parameter showed no mutagenic potential for these molecules.

3. Conclusions

A series of imidamide-based derivatives were designed and synthesized. They were screened for their inhibitory activity against the inducible and neuronal nitric oxide synthase (iNOS and nNOS). Four of them disclosed promising IC_{50} values for the iNOS inhibitory activity with values ranging from 4.6 to 107.6 μM, being the acetimidamide **9a** the best inhibitor, showing selectivity against iNOS. Molecular docking studies on **9a** suggest a particular binding mode that might explain its high iNOS selectivity, and that is based on a three-point H-bond coordination to the catalytically essential residue Glu377. Physicochemical parameters predicted good drug-like effects and promising pharmacokinetic profile for the best inhibitors. Furthermore, pharmacological experiments with aortic rat tissue confirmed that **9a** conserved its iNOS inhibitory activity at the tissue level. In addition, a total absence of eNOS inhibition was also observed in the range of concentrations in which **9a** is considered effective on iNOS, demonstrating the selectivity necessary to avoid the adverse effects of hypertension. Moreover, the cell viability test demonstrated the absence of cell toxicity in the imidamide derivatives **9a**, **9b**, **9e** and **9g** at their IC_{50} value. Accordingly, compound **9a** could be considered as a structural lead for further optimization to obtain more active iNOS inhibitors that would serve as new therapeutic alternatives in the treatment of diseases in which the inducible isoform is involved, such as septic shock.

4. Experimental section

4.1. Chemistry

4.1.1. General information

Reagents, deuterated solvents and common solvents were purchased from Sigma-Aldrich and Acros Organic. Nuclear magnetic resonance spectra were recorded in CD₃OD, CDCl₃ and (CD₃)₂SO with tetramethylsilane (TMS) as the internal standard using a Bruker Avance NEO spectrometers with Smart Probe BBFO equipped, operating at 400.57 MHz for ¹H and 100.73 MHz for ¹³C, at 499.79 MHz for ¹H and 125.68 MHz for ¹³C at room temperature (rt) in all cases. Chemicals shifts (δ) are reported in ppm and are referenced to the residual solvent peak, and coupling constants *J* are indicated in hertz (Hz). The following abbreviations are used to designate multiplicities: s = singlet, d = doublet, t = triplet, m = multiplet, dd = double-doublet, ddd = double-double-

doublet, dddd = double-double-double-doublet, dt = double-triplet, ddt = double-double-triplet and tt = triple-triplet. HRMS was conducted on a Waters LCT Premier Mass Spectrometer. Melting points were determined on an electrothermal melting point apparatus and were uncorrected. Analytical thin layer chromatography (TLC) was performed using Merck Kieselgel 60 F254 aluminium plates and visualised by UV light. All evaporations were carried out in vacuo in a Buchi rotary evaporator and the pressure controlled by a € Vacuubrand CVCII apparatus. Merck silicagel 60 (Merck, Kenilworth, NJ) with a particle size of 0.040–0.063 mm (230–400 mesh ASTM) was used for flash chromatography.

4.1.2. Synthesis of 3-Hydroxy-3-(pyridin-3-yl)propanenitrile 13 [36]

Working under anhydrous conditions, dry THF (20 mL) was introduced into a three-necked flask cooled down to −78 °C by a mixture of dry ice/acetone. Next, butyllithium (1.6 M/hexane, 12.5 mL) and acetonitrile (1.6 mL) were added carefully in order to maintain the temperature stable. The mixture was stirred for 1 h at −78 °C. After this time, a solution of nicotinaldehyde **6** (10 mmol) in anhydrous THF (10 mL) was added dropwise. During the next 30 min the reaction was stirred at −78 °C, right after this period, the dry ice/acetone bath was taken away, allowing the flask reach room temperature. The reaction was quenched with cold water (25 mL), and the solvent was evaporated. The crude mixture was purified by flash chromatography (EtOAc/hexane, 4:1), and 9.43 mmol (1.40 g) of an orange oil was obtained. Yield: 94%.

4.1.3. Synthesis of 3-amino-1-(pyridin-3-yl)propan-1-ol 14 [37]

Using a Schlenk line, 3-hydroxy-3-(pyridin-3-yl)propanenitrile **7** (2 mmol), dissolved in anhydrous THF (10 mL), was cannulated over suspended LiAlH$_4$ (7.5 mmol) in anhydrous THF (15 mL) at 0 °C. The reaction was stirred for 20 min, then it was neutralized by addition of 5 M NaOH solution (10 mL) and anhydrous Na$_2$SO$_4$ (600 mg) stirring for another 15 min. Filtration through celite allowed the retention of all solids, which were washed thoroughly with DCM/MeOH (7: 3). The filtrate was concentrated and the crude was used for the next step without further purification.

4.1.4. General method for the synthesis of the benzyl-benzimidothioates 15b-d

Commercially available benzothioamides (5 mmol) were dissolved in CHCl$_3$ (15 mL); then, benzyl bromide (5.5 mmol, 634 μl) was added and the mixture was refluxed for 2 h. After cooling, the resulting white solid was filtered under vacuum.

Benzylbenzimidothioate hydrobromide (**15b**) [38]. White solid; mp: 194–196 °C; 94% yield.

Benzyl 4-chlorobenzimidothioate hydrobromide (**15c**) [39]. White solid; mp: 182–184 °C; 90% yield.

Benzyl 4-(trifluoromethyl)benzimidothioate hydrobromide (**15d**) [24]. White solid; mp: 147–145 °C; 79% yield.

4.1.5. Synthesis of N-(3-hydroxy-3-(pyridin-3-yl)propyl)cyanamide 16

To a solution of 3-amino-1-(pyridin-3-yl)propan-1-ol **14** (2.09 mmol) in MeOH (10 mL), sodium acetate anhydrous (8.36 mmol) was added. The solvent was evaporated under vacuum. Once a dry solid was obtained, anhydrous MeOH (10 mL) was added under argon and the reaction mixture was cooled to 0 °C; then, BrCN (4.17 mmol) was added. The resulting mixture was stirred for 2 h at room temperature and the solvent was evaporated. The crude was purified by flash chromatography (DCM/MeOH, 9.5: 0.5). Orange oil; 85% yield.

^{1}H NMR (400 MHz, CD$_3$OD) δ 8.57 (s, 1H), 8.47 (d, J = 4.9 Hz, 1H), 7.90 (d, J = 7.9 Hz, 1H), 7.46 (dd, J = 7.9 Hz, J = 4.9 Hz, 1H), 4.85 (m, 1H), 3.26 – 3.13 (m, 2H), 2.01 – 1.95 (m, 2H). ^{13}C NMR (100 MHz, CD$_3$OD) δ 148.91, 147.89, 142.56, 135.99, 125.30, 124.41, 69.46, 43.45, 39.90. HRMS (LSIMS) *m/z* calcd for C$_9$H$_{12}$N$_3$O 178.0980 [M + H]$^+$; found: 178.0990.

4.1.6. N-(3-Hydroxy-3-(pyridin-3-yl)propyl)carbamimidic acid 17

After maintaining the cyanamide **10** in the presence of water, it was transformed into the carbamimidic acid **11**, that was purified by flash chromatography (DCM/MeOH, 8.5: 1.5). 93% yield.

^{1}H NMR (400 MHz, CD$_3$OD) δ 8.54 (s, 1H), 8.42 (d, J = 4.8 Hz, 1H), 7.86 (d, J = 7.5 Hz, 1H), 7.42 (dd, J = 7.5 Hz, J = 4.8 Hz, 1H), 4.78 (dd, J = 7.7 Hz, J = 5.4 Hz, 1H), 3.23 (ddt, J = 20.0 Hz, J = 13.3 Hz, J = 6.6 Hz, 2H), 1.88 (dt, J = 10.9 Hz, J = 7.3 Hz, 2H). ^{13}C NMR (100 MHz, CD$_3$OD) δ 162.38, 148.74, 147.98, 142.69, 135.94, 125.18, 70.21, 40.37, 37.90, 35.37. HRMS (LSIMS) *m/z* calcd for C$_9$H$_{13}$N$_3$O$_2$ 196.1008 [M + H]$^+$; found: 196.0943.

4.1.7. General method for the synthesis of N-(3-hydroxy-3-(pyridin-3-yl) propyl)imidamides 9a-d

To a solution of 3-amino-1-(pyridin-3-yl)propan-1-ol **14** (2 mmol) in MeOH (10 mL), cooled to 0 °C, the different imidates **15a-d** (3 mmol) [24] were added. The reaction mixture was stirred for 15 h at room temperature. After this time, the mixture was evaporated under vacuum and the crude was purified by flash chromatography (DCM/MeOH, 7: 3 saturating with NH$_4$OH).

N-(3-Hydroxy-3-(pyridin-3-yl)propyl)acetimidamide (**9a**). Yellow oil; 98% yield

^{1}H NMR (400 MHz, CD$_3$OD) δ 8.51 (d, J = 2.0 Hz, 1H), 8.40 (dd, J = 4.9 Hz, J = 2.0 Hz, 1H), 7.83 (dt, J = 8.0 Hz, J = 2.0 Hz, 1H), 7.32 (ddd, J = 8.0 Hz, J = 4.9 Hz, J = 0.9 Hz, 1H), 4.78 (dd, J = 8.6 Hz, 4.6 Hz, 1H), 3.48 – 3.29 (m, 2H), 2.13 (s, 3H), 2.02 – 1.92 (m, 2H). ^{13}C NMR (100 MHz, CD$_3$OD) δ 163.79, 148.04, 147.46, 140.92, 133.35, 123.30, 67.28, 38.89, 36.80, 18.47. HRMS (LSIMS) *m/z* calcd for C$_{10}$H$_{16}$N$_3$O: 194.1293 [M + H]$^+$; found: 194.1306.

N-(3-Hydroxy-3-(pyridin-3-yl)propyl)benzimidamide (**9b**). Yellow solid; mp: 178–180 °C; 80% yield

^{1}H NMR (500 MHz, CD$_3$OD) δ 8.65 (d, J = 2.0 Hz, 1H), 8.48 (dd, J = 4.9 Hz, J = 2.0 Hz, 1H), 7.98 (dt, J = 7.9 Hz, J = 2.0 Hz, 1H), 7.81 – 7.77 (m, 2H), 7.75 (tt, J = 7.5 Hz, J = 7.5 Hz, J = 1.3 Hz, J = 1.3 Hz, 1H), 7.66 – 7.61 (m, 2H), 7.48 (ddd, J = 7.9 Hz, J = 4.9 Hz, J = 0.9 Hz, 1H), 5.00 (dd, J = 9.1 Hz, J = 4.1 Hz, 1H), 3.78 – 3.66 (m, 2H), 2.29 – 2.14 (m, 2H). ^{13}C NMR (100 MHz, CD$_3$OD) δ 165.86, 149.06, 148.00, 142.18, 135.90, 134.66, 130.50, 130.39, 128.95, 125.26, 69.99, 41.54, 37.43. HRMS (LSIMS) *m/z* calcld for C$_{15}$H$_{18}$N$_3$O: 256.1450 [M + H]$^+$; found: 256.1445.

4-Chloro-N-(3-hydroxy-3-(pyridin-3-yl)propyl)benzimidamide (**9c**). White solid; mp: 200–202 °C; 82% yield

^{1}H NMR (400 MHz, CD$_3$OD) δ 8.61 (d, J = 2.2 Hz, 1H), 8.41 (dd, J = 4.9 Hz, J = 1.6 Hz, 1H), 7.94 (dddd, J = 7.9 Hz, J = 2.2 Hz, J = 1.6 Hz, J = 0.6 Hz, 1H), 7.77 (d, J = 8.9 Hz, 2H), 7.59 (d, J = 8.9 Hz, 2H), 7.42 (ddd, J = 8.0 Hz, J = 4.9 Hz, J = 0.6 Hz, 1H), 4.98 (dd, J = 9.1 Hz, J = 4.0 Hz, 1H), 3.75 – 3.62 (m, 2H), 2.26 – 2.10 (m, 2H). ^{13}C NMR (100 MHz, CD$_3$OD) δ 164.70, 148.90, 147.92, 142.06, 140.63, 135.92, 130.84, 130.49, 128.85, 125.21, 69.80, 41.64, 37.34. HRMS (LSIMS) *m/z* calcd for C$_{15}$H$_{17}$N$_3$OCl: 290.1060 [M + H]$^+$; found: 290.1059.

N-(3-Hydroxy-3-(pyridin-3-yl)propyl)-4-(trifluoromethyl)benzimidamide (**9d**). White solid; mp: 195–197 °C; 83% yield

^{1}H NMR (500 MHz, CD$_3$OD) δ 8.65 (d, J = 2.2 Hz, 1H), 8.49 (dd, J = 4.9 Hz, J = 1.6 Hz, 1H), 8.00 – 7.99 (m, 1H), 7.97 (q, J = 8.2 Hz, 4H), 7.49 (ddd, J = 7.8 Hz, J = 4.9 Hz, J = 0.8 Hz, 1H), 5.00 (dd, J = 9.0 Hz, J = 4.1 Hz, 1H), 3.84 – 3.64 (m, 2H), 2.37 – 2.10 (m, 2H). ^{13}C NMR (125 MHz, CD$_3$OD) δ 164.93, 149.12, 148.03, 142.21, 135.92, 135.74, 134.33, 130.14, 127.26, 125.29, 124.90, 69.96, 41.73, 37.36. HRMS (LSIMS) *m/z* calcd for C$_{16}$H$_{17}$N$_3$OF$_3$: 324.1324 [M + H]$^+$; found: 324.1298.

4.1.8. Synthesis of final dimer compounds 9e-g

((((3-Hydroxy-3-pyridin-3-yl)propyl)amino)(imino)methyl *N*-(3-hydroxy-3-pyridin-3-yl)propyl)imidocarbamate (**9e**).

To a solution of carbamimidic acid **17** (1.5 mmol) in DMSO (5 mL) under argon, was added sodium hydride (60%, 1.8 mmol) and the

mixture was stirred for 1 h at room temperature. Then, a solution of the cyanamide **16** (1 mmol) in DMSO (5 mL) was added dropwise. The mixture was further stirred for 24 h at room temperature. Then, the reaction was stopped by addition of ice, and the solvent was evaporated. The crude was purified by flash chromatograpy (DCM/MeOH, 9: 1). Orange oil. 76% yield.

^{1}H NMR (400 MHz, CD$_3$OD) δ 8.55 (s, 2H), 8.44 (d, J = 4.9 Hz, 2H), 7.87 (d, J = 7.9 Hz, 2H), 7.43 (dd, J = 7.9 Hz, J = 4.9 Hz, 2H), 4.79 (dd, J = 7.9 Hz, J = 5.4 Hz, 2H), 3.29 – 3.18 (m, 4H), 1.95 – 1.84 (m, 4H). ^{13}C NMR (100 MHz, CD$_3$OD) δ 162.40, 148.85, 148.08, 142.66, 135.83, 125.15, 70.29, 40.39, 37.95. HRMS (LSIMS) m/z calcd for C$_{18}$H$_{24}$N$_6$O$_3$ 373.1998 [M + H]$^+$; found: 373.1998.

Synthesis of 1,5-bis(3-hydroxy-3-(pyridin-3-yl)propyl)biguanidine (9f).

Working under argon atmosphere, the cyanamide **16** (3 mmol) was solved in DMF (7 mL), then 1 M NH$_3$ was added and the mixture was refluxed for 1 h. Afterward, 2 N NaOH (10 mL) was added. The mixture was evaporated to dryness. The crude was purified by flash chromatography (DCM/MeOH, 9: 1, saturating with NH$_4$OH. Orange oil; 68% yield.

^{1}H NMR (400 MHz, CD$_3$OD) δ 8.60 (s, 2H), 8.49 (d, J = 4.9 Hz, 2H), 7.91 (d, J = 7.8 Hz, 2H), 7.48 (dd, J = 7.8 Hz, J = 4.9 Hz, 2H), 4.94 (dd, J = 8.6 Hz, J = 4.2 Hz, 2H), 3.23 – 3.06 (m, 4H), 2.14 – 1.98 (m, 4H). ^{13}C NMR (100.63 MHz, CD$_3$OD) δ 170.17, 149.29, 147.93, 142.02, 135.70, 125.27, 70.85, 38.69, 36.96. HRMS (LSIMS): m/z calcd for C$_{18}$H$_{26}$N$_7$O$_2$ 372.2148 [M + H]$^+$; found: 372.2148.

Synthesis of 1,3-bis(3-hydroxy-3-(pyridin-3-yl)propyl)guanidine (9 g).

3-Amino-1-(pyridin-3-yl)propan-1-ol hydrochloride **14** (1.5 mmol) was solved in MeOH (5 mL) and 1 M HCl solution in ether (3 mL) was added. The mixture was stirred for about 15 min, and the solvent was evaporated under vacuum to dryness obtaining the aminopropanol hydrochloride. Next, working under argon atmosphere, a solution of cyanamide **16** (1 mmol) in ethanol (7 mL) was added to the aminopropanol hydrochloride **14** freshly prepared. The mixture was refluxed for 3 h. Then, the solvent was evaporated and the crude was purified by flash chromatography (DCM/MeOH, 8: 2, saturating with NH$_4$OH).Orange oil; 73% yield.

^{1}H NMR (400 MHz, (CD$_3$)$_2$SO) δ 8.67 (d, J = 1.8 Hz, 2H), 8.55 (dd, J = 5.0 Hz, J = 1.5 Hz, 2H), 8.02 (dd, J = 8.0 Hz, J = 1.9 Hz, 2H), 7.91 (t, J = 5.3 Hz, 2H), 7.55 (dd, J = 7.9 Hz, J = 5.0 Hz, 2H), 5.82 (s, 2H), 4.82 (dd, J = 8.8 Hz, J = 4.2 Hz, 2H), 3.36 – 3.19 (m, 4H), 1.95 – 1.75 (m, 4H). ^{13}C NMR (100 MHz, (CD$_3$)$_2$SO) δ 156.00, 147.52, 146.78, 141.15, 134.29, 123.68, 67.49, 38.23, 37.82. HRMS (LSIMS) m/z calcd for 330.1930 C$_{17}$H$_{24}$N$_5$O$_2$ [M + H]$^+$; found: 330.1931.

4.1.9. Synthesis of N-(3-oxo-3-(pyridin-3-yl)propyl)acetimidamide 10a

To a solution of *N*-(3-hydroxy-3-(pyridin-3-yl)propyl)acetimide **9a** (1 mmol) in H$_2$O (10 mL), sodium dichromate (0.5 mmol) was added. The mixture was cooled to 0 °C and then, a solution of 10 M sulfuric acid was added. The mixture was stirred for 16 h. Afterward, a saturated solution of NaHCO$_3$ (5 mL) was added and the water was evaporated under vacuum. The resulting salts were filtered and washed with methanol. The solvent was evaporated and the crude was purified by flash chromatography (DCM/MeOH, 8: 2 saturating with NH$_4$OH). White oil; 61% yield.

^{1}H NMR (500 MHz, CDCl$_3$) δ 9.17 (d, J = 1.7 Hz, 1H), 8.80 (dd, J = 4.8 Hz, J = 1.7 Hz, 1H), 8.22 (dt, J = 8.0 Hz, J = 1.7 Hz, 1H), 7.44 (dd, J = 8.0 Hz, J = 4.8 Hz, 1H), 6.12 (s, 1H), 3.69 (q, J = 5.8 Hz, 2H), 3.26 (t, J = 5.5 Hz, 2H), 1.96 (s, 3H). ^{13}C NMR (125 MHz, CDCl$_3$) δ 198.66, 170.35, 154.10, 149.78, 135.43, 131.82, 123.85, 38.72, 34.22, 23.47. HRMS (LSIMS) m/z calcd for C$_{10}$H$_{14}$N$_3$O 192.1137 [M + H]$^+$; found: 192.1128.

4.1.10. General method for the synthesis of 2-substituted-4-(pyridin-3-yl)pyrimidines 11a-d.

N-(3-hydroxy-3-(pyridin-3-yl)propyl)imidamide derivatives (**9a-d**) (1 mmol) were dissolved in acetonitrile (20 mL) under argon. Then, manganese dioxide (10 mmol) was added and the mixture was kept under strong stirring for 48 h. After this time, the reaction mixture was filtered through celite. The solvent was evaporated and the crude was purified by flash chromatography (DCM/MeOH, 9.5: 0.5).

2-Methyl-4-(pyridin-3-yl)pyrimidine (11a). White solid; mp: 89 – 90 °C °C; 83% yield.

^{1}H NMR (500 MHz, CDCl$_3$): δ 9.26 (s, 1H), 8.73 (d, J = 5.3 Hz, 2H), 8.42 (dt, J = 8.0 Hz, J = 1.9 Hz, 1H), 7.55 (d, J = 5.3 Hz.1H), 7.45 (dd, J = 8.0 Hz, J = 4.9 Hz, 1H), 2.82 (s, 3H). ^{13}C NMR (125 MHz, CDCl$_3$) δ 169.02, 161.85, 158.02, 151.76, 148.70, 134.85, 132.81, 123.93, 114.12, 26.41. HRMS (LSIMS) m/z calcdo for C$_{10}$H$_{10}$N$_3$ 172.0875 [M + H]$^+$; found: 172.0859.

2-Phenyl-4-(pyridin-3-yl)pyrimidine (11b) [28]. White solid; mp: 91 – 93 °C; 81% yield.

^{1}H NMR (400 MHz, CDCl$_3$): δ 9.40 (d, J = 1.7 Hz, 1H), 8.90 (d, J = 5.2 Hz, 1H), 8.77 (dd, J = 4.8 Hz, J = 1.7 Hz, 1H), 8.60–8.53 (m, 3H), 7.63 (d, J = 5.2 Hz, 1H), 7.55 – 7.51 (m, 3H), 7.49 (ddd, J = 8.0 Hz, J = 4.8 Hz, J = 0.9 Hz, 1H). ^{13}C NMR (100 MHz, CDCl$_3$) δ 165.09, 161.78, 158.41, 151.83, 148.75, 137.61, 134.84, 132.83, 131.16, 128.78, 128.48, 123.94, 114.69. HRMS (LSIMS) m/z calcd for 234.1031 C$_{15}$H$_{12}$N$_3$ [M + H]$^+$; found: 234.1025.

2-(4-Chlorophenyl)-4-(pyridin-3-yl)pyrimidine (11c) [28]. Yellow solid; mp: 151 – 153 °C; 80% yield. mp = 142–144 °C.

^{1}H NMR (400 MHz, CDCl$_3$): δ 9.39 (d, J = 1.0 Hz, 1H), 8.89 (d, J = 5.2 Hz, 1H), 8.78 (dd, J = 4.5 Hz, J = 0.9 Hz, 1H), 8.57–8.49 (m, 3H), 7.65 (d, J = 5.2 Hz, 1H), 7.54 – 7.47 (m, 3H). ^{13}C NMR (100 MHz, CDCl$_3$) δ 164.16, 161.90, 158.46, 151.93, 148.73, 137.43, 136.11, 134.83, 132.68, 129.83, 129.01, 123.97, 114.88. HRMS (LSIMS) m/z calcd for 268.0642 C$_{15}$H$_{11}$N$_3$Cl [M + H]$^+$; found: 268.0638.

4-(Pyridin-3-yl)-2-((4-trifluoromethyl)phenyl))pyrimidine (11d) [28]. White solid; mp: 155 – 156 °C; 85% yield.

^{1}H NMR (500 MHz, CDCl$_3$): δ 9.41 (d, J = 1.9 Hz, 1H), 8.92 (d, J = 5.2 Hz, 1H), 8.79 (dd, J = 4.9 Hz, J = 1.9 Hz, 1H), 8.68 (d, J = 8.3 Hz, 2H), 8.56 (dt, J = 8.0 Hz, J = 1.9 Hz, 1H), 7.77 (d, J = 8.3 Hz, 2H), 7.69 (d, J = 5.2 Hz, 1H), 7.53 (dd, J = 8.0 Hz, J = 4.9 Hz, 1H). ^{13}C NMR (125 MHz, CDCl$_3$) δ 163.76, 161.78, 158.61, 151.51, 148.29, 140.77, 135.22, 132.71, 132.69, 128.76, 125.68, 124.24, 124.15, 115.40. HRMS (LSIMS) m/z calcd for C$_{16}$H$_{11}$N$_3$F$_3$ 302.0905 [M + H]$^+$; found: 302.0929.

4.2. In vitro nNOS and iNOS activity determination

All final products were tested *in vitro* following a methodology based on the detection of β emissions from tritium nuclei.

By monitoring the conversion of L-[^{3}H]-arginine to L-[^{3}H]-citrulline, it was possible to determine the inhibition rate in NO production on both NOS isoforms.

Each measure for any compound or concentration was performed in triplicate in a buffer solution at pH 7.6 containing Tris-HCl [25 mM], DTT [1 mM], BH$_4$ [4 μM], FAD [10 μM], inosine [0.5 mM], BSA [0.5 mg/ml], CaCl$_2$ [0.1 mM], L-arginine [10 μM], calmodulin [10 μg/ml] (only in nNOS) and L-[^{3}H]-arginine [0.05 μM].

The general procedure for each replica goes as follows: 50 μl of buffer solution, 10 μl of the desired NOS isoform diluted to reach optimum activity for the study, 10 μl from a compound solution to be evaluated, 10 μl of NADPH [7.5 mM] and, finally, enough H$_2$O MiliQ for a final volume of 100 μl. The mixture is then incubated for 30 min at 37 °C in order to let the enzymatic reaction take place. Once this process is completed, 400 μl of cold stop buffer is added. This solution at pH 5.5 contains HEPES [0.1 M], EGTA [10 mM] and L-citrulline [0.175 mg/ml]. For the next stage, 100 μl out of the 500 μl from each replica are passed through a column filled with Dowex-50 W ion exchange resin (Na +),

which has to be washed twice with 600 μl of MiliQ H_2O. This process reduces the radioactivity by 98%. The last step consists in diluting 50 μl from the previous mixture in 4 mL of Eco Lite (+) scintillation liquid, which has to rest at least 24 h in the dark for measurement stabilization in a Beckman LS 6500 multi-purpose scintillation counter.

For these experiments, Enzo Life Sciences (Taper) provided the recombinant human isoforms of iNOS and nNOS, Amersham Biosciences (Perkin Elmer) produced L-[^{3}H]-arginine while all the other reagents were available at Sigma-Aldrich (Merk).

The statistical treatment of data was carried out thanks to Prism8 program (GraphPad), using non-linear regression ELISA studies with variable slope of four factors for the IC_{50} calculation.

4.3. Tissue preparation and measurement of tension

The investigation conforms to the Guide for the Care and Use of Laboratory Animals published by the US National Institutes of Health (NIH Publication No. 85–23, revised 1996) and with the principles outlined in the Declaration of Helsinki and approved by our institutional review board. Male Wistar rats (250–300 g), obtained from Harlam Laboratories SA (Barcelona, Spain), were euthanized by a quick blow on the head followed by exsanguination. The descending thoracic aortic rings were dissected, the endothelium was removed mechanically and incubated in Krebs solution (composition in mM: NaCl, 118; KCl, 4.75; $NaHCO_3$, 25; $MgSO_4$, 1.2; $CaCl_2$, 2; KH_2PO_4, 1.2; and glucose, 11) at 37 °C and gassed with 95% O_2 and 5% CO_2 for 20 h in a cell culture incubator in the absence or presence of *Escherichia coli* 055:B5 lipopolysaccharide (LPS, 1 μg/ml) (Sigma-Aldrich, Madrid, Spain). Rings were then mounted in organ chambers filled with Krebs solution and were stretched to 2 g of resting tension by means of two L-shaped stainless-steel wires inserted into the lumen and attached to the chamber and to an isometric force–displacement transducer (UF-1, Cibertec, Madrid, Spain), and recorded in a recording and analysis system (MacLab ADInstruments), as described previously by Romero et al. [40]. After equilibration of aortic rings, concentration–response curves for noradrenaline (NA, 10^{-9}-10^{-5} M) were performed by increasing the concentration in the organ chamber in cumulative increments after a steady-state response had been reached with each increment. Then, after washing, a second concentration–response curve was performed in rings preincubated with the no selective nitric oxide synthase (NOS) inhibitor, NG-nitro-L-arginine methylester (L-NAME, 300 μM), **9a** (5 μM), or its vehicle (DMSO, 1/10^6) were added to the organ chamber 30 min before the addition of NA. The rings were then removed from the organ chambers, air dried for 24 h, and weighed. The contraction was expressed in grams of force per milligram of dried tissue. The area under concentration–response curve (AUC) was measured.

In another experiments, aortic rings with a functional endothelium were incubated with L-NAME (100 μM), **9a** (5 μM), or its vehicle (DMSO, 1/10^6) for 30 min, and contracted with NA (1 μM). Once a plateau contraction was reached, a concentration–response curve was constructed by cumulative addition of acetylcholine. Results are expressed as percentage of NA-evoked contraction. Data are expressed as means ± standard error mean and n reflects the number of aortic rings from different rats. Statistically significant differences among groups were calculated by two-way ANOVA followed by a Dunnett's multiple comparison test. P < 0.05 was considered statistically significant.

4.4. Cell viability assay

To examine the cytotoxicity induced by compounds **9a**, **9b**, **9e** and **9g**, we evaluated the cell viability activity of these compounds using human umbilical vein endothelial cells (HUVECs) by the MTT reduction assay [24]. Briefly, HUVECs were seeded at 1x10^4 cells per well in a 96-well microtiter plate and incubated at 37 °C for up to 24 h. Then, the cells supernatants were removed and replaced by fresh medium serum free for at least two hours before the cells were exposed to serial dilutions of compounds (10–500 μM) for 30 min. At the selected time, 20 uL of 5 mg/ml MTT in PBS was added to the cells and further incubated at 37 °C for 3 h. After washing, 100 μl of DMSO were added into each well, and the spectrophotometric analysis was run at 570 nm using a multi-well plate reader (Fluorostart; BMG Labtechnologies, Offenburg, Germany) with background subtraction at 630 nm. Cell viability was calculated as the percentage of the viable cells compared with untreated controls. The viability experiments were conducted in at least three independent times, each run in triplicate. Results are expressed as percentage relatively to the untreated condition.

4.5. Docking protocol

Docking studies were carried out with Autodock 4.2.6 (AD4) [41] on the iNOS and nNOS pdb IDs 4CX7 and 6AV2 respectively. Ligands structures were built on Avogadro [42] and optimized using Gaussian [43] (HF/6-31G(d,p)). Compounds presenting tertiary amines, prone to protonation at physiological pH, were also considered. Once optimized, ligands PDBs were prepared for docking using the prepare_ligand4.py script included MGLTools 1.5.4 [41]. Protein structures, on the other hand, were prepared for docking using the PDB2PQR tools [44]. Water and ligand molecules were removed and charges and non-polar hydrogen atoms were added at pH 7.0. The produced structures were saved as a pdb files and prepared for docking using the prepare_receptor4.py script from MGLTools. The Fe atom of heme was assigned a charge of +3. AD4 was used to automatically dock the ligands into the iNOS and nNOS binding sites. For both enzymes, the docking grid was centered on the ligand binding site and set with the following grid parameters: 60 Å × 60 Å × 60 Å with 0.375 Å spacing. In all calculations, AD4 parameter file was set to 100 GA runs, 2.500.000 energy evaluations and a population size of 150. The Lamarckian genetic algorithm local search (GALS) method was used for the docking calculations. All dockings were performed with a population size of 250 and a Solis and Wets local search of 300 rounds was applied with a probability of 0.06. A mutation rate of 0.02 and a crossover rate of 0.8 were used. The docking results from each of the 100 calculations were clustered based on root-mean square deviation (RMSD) solutions differing by less than 2.0 Å between the Cartesian coordinates of the atoms and ranked on the basis of free energy of binding. The obtained conformations were individually inspected and the best performing poses in terms of energy were selected. UCSF Chimera 1.15 was used to analyse the obtained conformations and generate the final figures [45].

Declaration of Competing Interest

The authors declare that they have no known competing financial interests or personal relationships that could have appeared to influence the work reported in this paper.

Appendix A. Supplementary material

Supplementary data to this article can be found online at https://doi.org/10.1016/j.bioorg.2022.105637.

References

[1] P. Picón-Pagès, J. Garcia-Buendia, F.J. Muñoz, Functions and dysfunctions of nitric oxide in brain, BBA – Mol. Basis Disease 1865 (8) (2019) 1949–1967, https://doi.org/10.1016/j.bbadis.2018.11.007.

[2] L.i. Zhou, D.-Y. Zhu, Neuronal nitric oxide synthase: structure, subcellular localization, regulation, and clinical implications, Nitric Oxide - Biol. Chem. 20 (4) (2009) 223–230, https://doi.org/10.1016/j.niox.2009.03.001.

[3] R. Rafikov, F.V. Fonseca, S. Kumar, D. Pardo, C. Darragh, S. Elms, D. Fulton, S. M. Black, eNOS activation and NO function: structural motifs responsible for the posttranslational control of endothelial nitric oxide synthase activity, J. Endocrinol. 210 (2011) 271–284, https://doi.org/10.1530/JOE-11-0083.

[4] M.A. Cinelli, H.T. Do, G.P. Miley, R.B. Silverman, Inducible nitric oxide synthase: regulation, structure, and inhibition, Med. Res. Rev. 40 (1) (2020) 158–189, https://doi.org/10.1002/med.21599.

[5] S. Anavi, O. Tirosh, iNOS as a metabolic enzyme under stress conditions, Free Radic. Biol. Med. (2019) 1–20, https://doi.org/10.1016/j.freeradbiomed.2019.10.411.

[6] D.D. Thomas, L.A. Ridnour, J.S. Isenberg, W. Flores-Santana, C.H. Switzer, S. Donzelli, P. Hussain, C. Vecoli, N. Paolocci, S. Ambs, C.A. Colton, C.C. Harris, D. D. Roberts, D.A. Wink, The chemical biology of nitric oxide: implications in cellular signaling, Free Radic. Biol. Med. 45 (1) (2008) 18–31, https://doi.org/10.1016/j.freeradbiomed.2008.03.020.

[7] U. Förstermann, T. Münzel, Endothelial nitric oxide synthase in vascular disease: from marvel to menace, Circulation 113 (13) (2006) 1708–1714, https://doi.org/10.1161/CIRCULATIONAHA.105.602532.

[8] R.F. Nasyrova, D.V. Ivashchenko, M.V. Ivanov, N.G. Neznanov, Role of nitric oxide and related molecules in schizophrenia pathogenesis: biochemical, genetic and clinical aspects, Front. Physiol. 6 (2015), https://doi.org/10.3389/fphys.2015.00139.

[9] J.E. Yuste, E. Tarragon, C.M. Campuzano, F. Ros-Bernal, Implications of glial nitric oxide in neurodegenerative diseases, Front. Cell. Neurosci. 9 (2015) 322, https://doi.org/10.3389/fncel.2015.00322.

[10] N. Zhang, Y. Diao, R. Hua, J. Wang, S. Han, J. Li, Y. Yin, Nitric oxide-mediated pathways and its role in the degenerative diseases, Front. Biosci. Landmark. 22 (2017) 824–834, https://doi.org/10.2741/4519.

[11] L. Hannibal, Nitric oxide homeostasis in neurodegenerative diseases, Curr. Alzheimer Res. 13 (2) (2016) 135–149, https://doi.org/10.2174/1567205012666150921101250.

[12] A.K. Halder, A. Mukherjee, N. Adhikari, A. Saha, T. Jha, Nitric oxide synthase (NOS) inhibitors in cancer angiogenesis, Curr. Enzym. Inhib. 12 (2015), https://doi.org/10.2174/1573408012666151126185456.

[13] D.A. Geller, T.R. Billiar, Molecular biology of nitric oxide synthases, Can. Metastasis Rev. 17 (1998) 7–23, https://doi.org/10.1023/A:1005940202801.

[14] A.A. Pradhan, Z. Bertels, S. Akerman, Targeted nitric oxide synthase inhibitors for Migraine, Neurotherapeutics. 15 (2) (2018) 391–401, https://doi.org/10.1007/s13311-018-0614-7.

[15] M.A. Titheradge, Nitric oxide in septic shock, Biochim. Biophys. Acta - Bioenerg. 1411 (2-3) (1999) 437–455, https://doi.org/10.1016/S0005-2728(99)00031-6.

[16] R.P. Dellinger, M.M. Levy, J.M. Carlet, J. Bion, M.M. Parker, R. Jaeschke, K. Reinhart, D.C. Angus, C. Brun-Buisson, R. Beale, T. Calandra, J.-F. Dhainaut, H. Gerlach, M. Harvey, J.J. Marini, J. Marshall, M. Ranieri, G. Ramsay, J. Sevransky, B.T. Thompson, S. Townsend, J.S. Vender, J.L. Zimmerman, J.-L. Vincent, Surviving sepsis campaign: international guidelines for management of severe sepsis and septic shock: 2008, Intensive Care Med. 34 (1) (2008) 17–60, https://doi.org/10.1007/s00134-007-0934-2.

[17] F. Daviaud, D. Grimaldi, A. Dechartres, J. Charpentier, G. Geri, N. Marin, J. D. Chiche, A. Cariou, J.P. Mira, F. Pène, Timing and causes of death in septic shock, Ann. Intensive Care. 5 (16) (2015) 1–19, https://doi.org/10.1186/s13613-015-0058-8.

[18] T.W.L. Scheeren, J. Bakker, D. De Backer, D. Annane, P. Asfar, E.C. Boerma, M. Cecconi, A. Dubin, M.W. Dünser, J. Duranteau, A.C. Gordon, O. Hamzaoui, G. Hernández, M. Leone, B. Levy, C. Martin, A. Mebazaa, X. Monnet, A. Morelli, D. Payen, R. Pearse, M.R. Pinsky, P. Radermacher, D. Reuter, B. Saugel, Y. Sakr, M. Singer, P. Squara, A. Vieillard-Baron, P. Vignon, S.T. Vistisen, I.C.C. van der Horst, J.L. Vincent, J.L. Teboul, Current use of vasopressors in septic shock, Ann. Intensive Care. 9 (20) (2019) 1–12, https://doi.org/10.1186/s13613-019-0498-7.

[19] L.C. López-Cara, M.D. Carrión, A. Entrena, M.A. Gallo, A. Espinosa, A. López, G. Escames, D. Acuña-Castroviejo, M.E. Camacho, 1,3,4-Thiadiazole derivatives as selective inhibitors of iNOS versus nNOS: synthesis and structure-activity dependence, Eur. J. Med. Chem. 50 (2012) 129–139, https://doi.org/10.1016/j.ejmech.2012.01.047.

[20] M.E. Camacho, J. Leon, A. Entrena, G. Velasco, M.D. Carrión, G. Escames, A. Vivo, D. Acuña-Castroviejo, M.A. Gallo, A. Espinosa, 4,5-Dihydro-1*H*-pyrazole derivatives with inhibitory nNOS activity in rat brain: synthesis and structure-activity relationships, J. Med. Chem. 47 (2004) 5641–5650.

[21] M.D. Carrión, M. Chayah, A. Entrena, A. López, M.A. Gallo, D. Acuña-Castroviejo, M.E. Camacho, Synthesis and biological evaluation of 4,5-dihydro-1*H*-pyrazole derivatives as potential nNOS/iNOS selective inhibitors. Part 2: Influence of diverse substituents in both the phenyl moiety and the acyl group, Bioorg. Med. Chem. 21 (14) (2013) 4132–4142, https://doi.org/10.1016/j.bmc.2013.05.016.

[22] M. Chayah, M.D. Carrión, M.A. Gallo, R. Jiménez, J. Duarte, M.E. Camacho, Development of urea and thiourea kynurenamine derivatives: synthesis, molecular modeling, and biological evaluation as nitric oxide synthase inhibitors, ChemMedChem 10 (5) (2015) 874–882, https://doi.org/10.1002/cmdc.201500007.

[23] M. Chayah, M.E. Camacho, M.D. Carrión, M.A. Gallo, M. Romero, J. Duarte, *N, N′*-Disubstituted thiourea and urea derivatives: design, synthesis, docking studies and biological evaluation against nitric oxide synthase, MedChemComm 7 (4) (2016) 667–678.

[24] F. Arias, F. Franco-Montalban, M. Romero, M.D. Carrión, M.E. Camacho, Synthesis, bioevaluation and docking studies of new imidamide derivatives as nitric oxide synthase inhibitors, Bioorg. Med. Chem. 44 (2021) 116294, https://doi.org/10.1016/j.bmc.2021.116294.

[25] J.A. Lowe, W. Qian, R.A. Volkmann, S. Heck, J. Nowakowski, R. Nelson, C. Nolan, D. Liston, K. Ward, S. Zorn, C. Johnson, M. Vanase, W.S. Faraci, A. Verdries, J. Baxter, S. Doran, M. Sanders, M. Ashton, P. Whittle, M. Stefaniak, A new class of selective and potent inhibitors of neuronal nitric oxide synthase, Bioorg. Med. Chem. Lett. 9 (17) (1999) 2569–2572.

[26] F. Xue, J. Fang, S.L. Delker, H. Li, P. Martásek, L.J. Roman, T.L. Poulos, R. B. Silverman, Symmetric double-headed aminopyridines, a novel strategy for potent and membrane-permeable inhibitors of neuronal nitric oxide synthase, J. Med. Chem. 54 (7) (2011) 2039–2048, https://doi.org/10.1021/jm101071n.

[27] W.K. Hagmann, C.G. Caldwell, P. Chen, P.L. Durette, C.K. Esser, T.J. Lanza, I. E. Kopka, R. Guthikonda, S.K. Shah, M. MacCoss, R.M. Chabin, D. Fletcher, S. K. Grant, Barbara G. Green, John L. Humes, Theresa M. Kelly, Sylvie Luell, R. Meurer, V. Moore, S.G. Pacholok, T. Pavia, H.R. Williamsc, K.K. Wong, 2-Aminopyridines as inhibitors of nitric oxide synthases, Bioorg. Med. Chem. Lett. 10 (2000) 1975–1978.

[28] W.J. Scott, W. Fu, M. Monahna, D. Bierer. Preparation of substituted 3-pyridyl pyrimidines as C17,20 lyase inhibitors. Pat No WO 03/027100 A1 (2003) DC: U.S. Patent and Trademark Office.

[29] P.L. Menna, D.F. Alonso, D.E. Gómez, J. Comin. Phenyl-guanidine derivatives. *Pat No US 9,745,257 B2*. 2017: Washington, DC: U.S. Patent and Trademark Office.

[30] M.-H. Liao, C.-C. Shih, C.-M. Tsao, S.-J. Chen, C.-C. Wu, A. Cignarella, RhoA/Rho-kinase and nitric oxide in vascular reactivity in rats with endotoxaemia, PLoS ONE 8 (2) (2013) e56331.

[31] C.M. Wong, C.L. Au, S.Y. Tsang, C.W. Lau, X. Yao, Z. Cai, A.C. Chung, Role of inducible nitric oxide synthase in endothelium-independent relaxation to raloxifene in rat aorta, Br. J. Pharmacol. 174 (8) (2017) 718–733, https://doi.org/10.1111/bph.13733.

[32] C. Liu, C.Y. Ngai, Y. Huang, W.H. Ko, M. Wu, G.W. He, C.J. Garland, K.A. Dora, X. Yao, Depletion of intracellular Ca^{2+} stores enhances flow-induced vascular dilatation in rat small mesenteric artery, Br J Pharmacol. 147 (5) (2006) 506–515, https://doi.org/10.1038/sj.bjp.0706639.

[33] H. Li, J. Jamal, S. Delker, C. Plaza, H. Ji, Q. Jing, H.e. Huang, S. Kang, R. B. Silverman, T.L. Poulos, The mobility of a conserved tyrosine residue controls isoform-dependent enzyme-inhibitor interactions in nitric oxide synthases, Biochemistry 53 (32) (2014) 5272–5279, https://doi.org/10.1021/bi500561h.

[34] E.D. Garcin, A.S. Arvai, R.J. Rosenfeld, M.D. Kroeger, B.R. Crane, G. Andersson, G. Andrews, P.J. Hamley, P.R. Mallinder, D.J. Nicholls, S.A. St-Gallay, A.C. Tinker, N.P. Gensmantel, A. Mete, D.R. Cheshire, S. Connolly, D.J. Stuehr, A. Åberg, A. V. Wallace, J.A. Tainer, E.D. Getzoff, Anchored plasticity opens doors for selective inhibitor design in nitric oxide synthase, Nat. Chem. Biol. 4 (11) (2008) 700–707, https://doi.org/10.1038/nchembio.115.

[35] D.E.V. Pires, T.L. Blundell, D.B. Ascher, pkCSM: Predicting small-molecule pharmacokinetic and toxicity properties using graph-based signatures, J. Med. Chem. 58 (9) (2015) 4066–4072, https://doi.org/10.1021/acs.jmedchem.5b00104.

[36] O. Pàmies, J.E. Bäckvall. Efficient Lipase-Catalyzed Kinetic Resolution and Dynamic Kinetic Resolution of β-Hydroxy Nitriles. A Route to Useful Precursors for γ-Amino Alcohols. Adv. Synth.Catal. 343 (6-7) (2001) 726-731. https://doi.org/10.1002/1615-4169(200108)343:6/7<726::AID-ADSC726>3.0.CO;2-E.

[37] M. Virgili-Bernado, M. Alonso-Xalma, C. Almansa-Rosales, J.L. Diaz-Fernandez. Preparation of meta-substituted phenylpyrazolo- and phenylpyrrolo-pyridazine derivatives with multimodal activity against pain. U.S. Patent Application (2020) No. 16/464,345.

[38] B.G. Shearer, J.A. Oplinger, S. Lee, S-2-Naphthylmethyl thioacetimidate hydrobromide: a new odorless reagent for the mild synthesis of substituted acetamidines, Tetrah. Lett. 38 (2) (1997) 179–182, https://doi.org/10.1016/S0040-4039(96)02268-X.

[39] L. Varoli, S. Burnelli, L. Garuti, B. Vitali, Synthesis and antimicrobial activity of new diazoimidazole derivatives containing an *N*-acylpyrrolidine ring, Il Farmaco 56 (11) (2001) 885–890.

[40] M. Romero, M. Toral, M. Gómez-Guzmán, R. Jiménez, P. Galindo, M. Sánchez, M. Olivares, J. Gálvez, J. Duarte, Antihypertensive effects of oleuropein-enriched olive leaf extract in spontaneously hypertensive rats, Food Funct. 7 (1) (2016) 584–593.

[41] G.M. Morris, R. Huey, W. Lindstrom, M.F. Sanner, R.K. Belew, D.S. Goodsell, A. J. Olson, AutoDock4 and AutoDockTools4: Automated docking with selective receptor flexibility, J. Comput. Chem. 30 (16) (2009) 2785–2791, https://doi.org/10.1002/jcc.21256.

[42] M.D. Hanwell, D.E. Curtis, D.C. Lonie, T. Vandermeersch, E. Zurek, G.R. Hutchison, Avogadro: an advanced semantic chemical editor, visualization, and analysis platform, J. Cheminf. 4 (2012) 17, https://doi.org/10.1186/1758-2946-4-17.

[43] M.J. Frisch, G.W. Trucks, H.B. Schlegel, G.E. Scuseria, M.A. Robb, J.R. Cheeseman, G. Scalmani, V. Barone, B. Mennucci, G.A. Petersson, H. Nakatsuji, M. Caricato, X. Li, H.P. Hratchian, A.F. Izmaylov, J. Bloino, G. Zheng, J.L. Sonnenberg, M. Hada, M. Ehara, K. Toyota, R. Fukuda, J. Hasegawa, M. Ishida, T. Nakajima, Y. Honda, O. Kitao, H. Nakai, T. Vreven, J.A. Montgomery, Jr., J.E. Peralta, F. Ogliaro, M. Bearpark, J.J. Heyd, E. Brothers, N. Kudin, V.N. Staroverov, T. Keit, R. Kobayashi, J. Normand, K. Raghavachari, A. Rendell, J.C. Burant, S.S. Iyengar, J. Tomasi, M.

Cossi, N. Rega, J.M. Millam, M. Klene, J.E. Knox, J.B. Cross, V. Bakken, C. Adamo, J. Jaramillo, R. Gomperts, R.E. Stratmann, O. Yazyev, A.J. Austin, R. Cammi, C. Pomelli, J.W. Ochterski, L. Martin, K. Morokuma, V.G. Zakrzewski, G.A. Voth, P. Salvador, J.J. Dannenberg, S. Dapprich, A.D. Daniels, O. Farkas, J.B. Foresman, J. V. Ortiz, J. Cioslowski, D.J. Fox, GAUSSIAN 09 (Revision D.1), GAUSSIAN 09 (Revision B.01). (2010).

[44] T.J. Dolinsky, J.E. Nielsen, J.A. McCammon, N.A. Baker, PDB2PQR: an automated pipeline for the setup of Poisson-Boltzmann electrostatics calculations, Nucleic Acids Res. 32 (Web Server) (2004) W665–W667, https://doi.org/10.1093/nar/gkh381.

[45] E.F. Pettersen, T.D. Goddard, C.C. Huang, G.S. Couch, D.M. Greenblatt, E.C. Meng, T.E. Ferrin, UCSF Chimera – a visualization system for exploratory research and analysis, J. Comput. Chem. 25 (13) (2004) 1605–1612, https://doi.org/10.1002/jcc.20084.